19th Brazilian Congress of Thermal Sciences and Engineering
November 6th–10th, 2022, Bento Gonçalves - RS - Brazil

ENC-2022-0139
NUMERICAL SIMULATION OF THE PARTICLE DISTRIBUTION AND ITS EFFECT ON THE APPARENT VISCOSITY OF NON-COLLOIDAL SUSPENSIONS

Nezia de Rosso
Cezar O. R. Negrão
Federal University of Technology-Paraná – UTFPR, Postgraduate Program in Mechanical and Materials Engineering – PPGEM, Research Center for Rheology and Non-Newtonian Fluids – CERNN, 81280-340, R. Deputado Heitor Alencar Furtado, 5000, Bloco N - Ecoville, Curitiba, PR, Brazil
nezia.rosso@gmail.com, negrao@utfpr.edu.br

Abstract. *The current work puts forward a numerical study of a non-colloidal suspension flows in three different rheometer geometries. The inhomogeneous Euler-Euler model applied to the continuity and momentum equations is used to solve the suspension flow problem. To save computational time, the numerical domain is reduced to an extension of 1 deg in the azimuthal direction by setting rotational periodic conditions as the boundaries. The objective is to investigate the effect of shear rate and geometry in the suspensions flow and its consequence on the measured apparent viscosity. Good agreement was obtained between literature and computed apparent viscosity. Analysis of particle distribution reveals that not only the particle motion but also the apparent viscosity depends on the shear rate and the geometry. Comparisons between geometries are performed to understand the reasons behind the particle motion. Numerical simulations are conducted using common rheometer geometries, such as cone-plate, rotational parallel plate and concentric cylinders. Other parameters are also investigated, namely particle volume fraction (from 0.1 to 0.5), and shear rates (from 10^{-3} to 5^{+2} s^{-1}). It can be anticipated that the heterogeneous particle distribution throughout the geometries is the main cause of differences on the calculated apparent viscosity.*

Keywords: *Suspension flow, Particle motion, Apparent viscosity, Euler-Euler, Simulation*

1. INTRODUCTION

Suspensions are multiphase substances composed of solid particles dispersed in a continuum. They are found in many industrial application such as pharmaceutics, food, construction, petroleum industry and in nature. Suspension behavior may be affected both by media composition as well as the way the continuum and dispersed phase interact. The interaction between the phases is the main responsible for phase distribution in the flow. Due to this interaction, even suspensions that have particle density identical to the liquid can present heterogeneity and make the characterization difficult.

Distinct behavior showed by suspension hinder their rheological characterization, and even suspension composed of Newtonian fluid and solid spherical particles may show different values of macroscopic properties, for example viscosity. As observed in literature (Lewis and Nielsen, 1968; Zarraga *et al.*, 2000; Denn *et al.*, 2018) suspension viscosity increase with particle volume fraction. However, such behavior may vary both as a function of physical characteristic (Mueller *et al.*, 2009; Gamonpilas *et al.*, 2016; Pednekar *et al.*, 2018) as well as the operating condition to which the sample is subject (Kulkarni and Morris, 2008; Linares-Guerrero *et al.*, 2017).

The particle distribution within the flow has been studied in pressure-driven flows (Nott and Brady, 1994; Tehrani, 1996), drag flows or a combination of both of them. The usual geometries used to characterize suspension drag flow are: cone-plate (CP) (Morris and Boulay, 1999; Gamonpilas *et al.*, 2016), parallel-plate (PP) (Zarraga *et al.*, 2000; Dai *et al.*, 2013; Gamonpilas *et al.*, 2016) and concentric cylinders (CC) (Abbott *et al.*, 1991; Huang and Bonn, 2007; Fall *et al.*, 2010).

Particle distribution is governed by either diffusion or convection that depend on the magnitude of the Reynolds numbers. While driven by diffusion (Eckstein *et al.*, 1977; Husband and Gadala-Maria, 1987; Wang *et al.*, 1996) in low Reynolds numbers ($Re \ll 1$) flows, particle motion is very much dependent on inertia forces in large Re flows (Matas *et al.*, 2004; Majji and Morris, 2018; Liu and Wu, 2019).

In particular, at low Reynolds numbers flows particle motion is named as particle migration and occur from regions of

high shear rate to regions of low shear rate in concentric cylinders. According to Leighton and Acrivos (1987); Acrivos *et al.* (1993) particle migration are induced by shear rate and are proportional to the square of the particle radius and the shear rate. Abbott *et al.* (1991); Chow *et al.* (1994); Husband *et al.* (1994); Konijn *et al.* (2014) noted that this particle migration cause a decrease in the suspension apparent viscosity. Other important observation was done by Fall *et al.* (2010), where authors noted that heterogeneity caused by particle motion is irreversible, means that particles do not return to the initial condition when the flow changes direction. Studies carried out in rotational parallel-plate geometry (PP) demonstrate that particles tend to migrate from regions of low shear rates, close to the center of the plates, to regions of high shear rates, close to the periphery of the plates (Krishnan *et al.*, 1996; Merhi *et al.*, 2005; Kim *et al.*, 2008). This migration was attributed to the curvature of the disk Krishnan *et al.* (1996); Shauly *et al.* (1998); Kim *et al.* (2008). This contradicts, therefore, the proposal of Leighton and Acrivos (1987); Acrivos *et al.* (1993) which assert that the particles should migrate to the region of low shear rate in the center of the plates due to the shear rate gradient. On the other hand, Morris and Boulay (1999) attributed the particle migration to the normal stresses generated by shear in non-homogeneous flows.

An important fact related to particle heterogeneity is how this affects the values of viscosity. Chapman and Leighton Jr (1991); Chow *et al.* (1994) noted a decrease in the suspension apparent viscosity with shear rate. Nevertheless, the authors were unable to identify particle migration in the radial direction. Chapman and Leighton Jr (1991) attributed the decrease in viscosity to sedimentation while Chow *et al.* (1994) attributed the decrease to a thin liquid layer close to the plates. On the other hand, Merhi *et al.* (2005); Fall *et al.* (2010) observed an increase in torque and, consequently, in the suspension apparent viscosity. The increase in torque was attributed to the increase in the particle volume fraction in the outer region of plates due to particle migration.

The works of Moon *et al.* (2015); Tanner and Dai (2016); Tanner (2018, 2020) assert that the particle migration has no effect on reducing viscosity and attribute the decrease of apparent viscosity to friction reduction between particles with increased in shear rate.

This shows that there is no consensus on the effect of the heterogeneity of particles in the suspension viscosity. In addition, it is not clear what mechanisms are responsible for particle motion in geometries used for the rheological characterization of suspensions, neither the effect of operating conditions in the observed trends. For Denn and Morris (2014), to understand the mechanisms behind particle migration and the irreversibility due to particle motion is the first step to predict rheology in complex flows.

The present work aims to study numerically particle motion of non-colloidal suspensions flows. The numerical study is conducted in domains that represent geometries usually used in the rheological characterization of suspensions. The Euler-Euler model is used to solve the two-phase liquid-solid flow that characterize the suspension flow. In general, it is sought to explore numerical results in order to understand the mechanisms associated with particle motion in the geometries of interest, under different operating conditions. Additionally, the work expects to contribute to the understanding of effect of particle motion on the apparent viscosity of the suspension.

2. NUMERICAL MODELING

Three different geometries were chosen to evaluate the effects of particle motion on the apparent viscosity. The first one is a cone-plate assembly, the second is a circular parallel-plates configuration and the last one is a concentric cylinders coupling, as illustrated in fig. 1. The cone-plate geometry, as the name suggests, is composed by a plate and a cone with equal radius R, that make an angle of 2 deg between each other, as one can see in the figure 1 a). The second geometry is a circular parallel-plates of radius R, separated by a distance H_p, as represented in figure 1 b). The sample, in both cone-plate and parallel-plates geometries, is held in place by the surface tension. The concentric cylinders, as illustrated in figure 1 c), consists of two cylinders of height H_c, concentric one with respect to each other and separated by a gap that is the difference between the outer and the inner radius, R_o and R_i respectively. All three domain are defined similarly by three walls: cone and lower plate, upper and lower plates, and outer and inner cylinders, and the fluid-ambient interface. A non-slip condition for the liquid phase is assumed for all walls (cone, plates and cylinders), while a free-slip condition is considered on the fluid-ambient wall, since the shear stress between the liquid and the outer environment air is negligible. For the solid dispersed phase, all walls are assumed as free-slip as suggested by ANSYS Inc. (2019). As an initial condition, the dispersed phase is considered to be homogeneously distributed throughout the domain.

2.1 Governing equations

The inhomogeneous Euler-Euler model, also known as the two-fluid model (Ishii and Hibiki, 2010), is used to solve the suspension flow in all three domains. The approach assumes average properties for both phases within a control volume weighted by the corresponding volume fraction of each phase. The average transport equations are combined with constitutive equations that account for the interactions between phases, represented by body and surface forces due to the momentum exchanged between the phases (Shi and Rzehak, 2020). Details of the model can be found in ANSYS Inc. (2019) and Yeoh and Tu (2019).

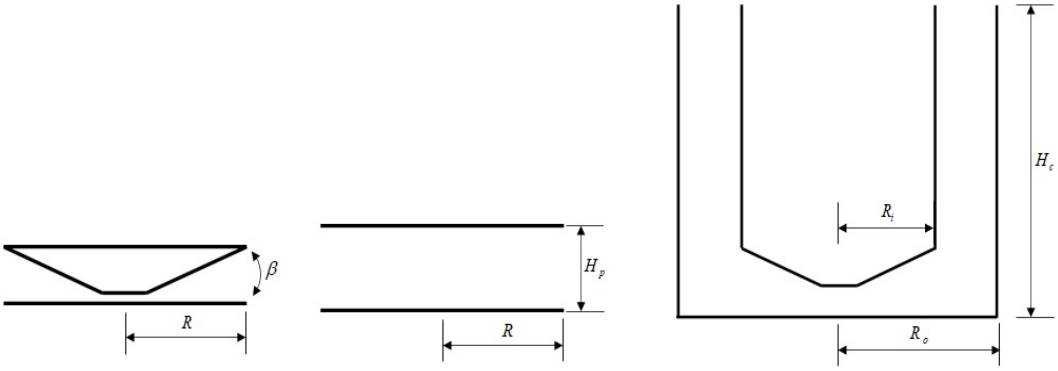

Figure 1. Schematic of three most usual geometries used in rotational rheometers. a) Cone-plate geometry, b) Parallel-plates geometry, and c) Concentric cylinders geometry

The governing equations, the continuity and momentum equations, valid for incompressible flows are considering in this work for two generic phases *i* $(i = s, l)$ in the framework of the two-fluid model, and are written in their canonical form as,

$$\frac{\partial(\alpha_i \rho_i)}{\partial t} + \nabla(\alpha_i \rho_i \vec{V_i}) = 0 \tag{1}$$

$$\frac{\partial(\alpha_i \rho_i \vec{V_i})}{\partial t} + \nabla(\alpha_i \rho_i \vec{V_i} \vec{V_i}) = -\nabla \alpha_i(p) + \alpha_i \mu_i \nabla^2 \vec{V_i} + \vec{M_i} \tag{2}$$

where the variables i represents the solid, s, or liquid, l, phase, α_i is the volume fraction of phase i, p is the pressure, $\vec{V_i}$ is the velocity vector of each phase, and the vector $\vec{M_i}$ represents the momentum produced on phase i by the stresses acting on the interface between the phases. The latter is modeled as a linear superposition of different interphase forces due to distinct solid-liquid interactions.

The interaction forces considered in the current case - the drag, the virtual mass and the lift forces - are represented in eq. 3. The drag force acts opposite to the relative motion between the particle and the surrounding media. The virtual mass force accounts for the added force a particle is due when accelerating or decelerating through a liquid, because of the mass of liquid it has to displace in this process. In turn, lift force acts perpendicular to the relative motion due to a velocity gradient in the continuous phase.

$$\vec{M_i} = \vec{M_s} = -\vec{M_l} = \alpha_s \left[\vec{f_D} + \vec{f_{VM}} + \vec{f_L} \right] \tag{3}$$

where $\vec{f_D}$, $\vec{f_{VM}}$ and $\vec{f_L}$ are the drag, virtual mass and lift forces per unit of volume of the rigid spheres and α_s is the solid volume fraction. The interphase forces satisfy the Newton's third law, as the liquid phase force magnitude acting upon the solid phase is identical to the solid force over the liquid phase with the opposite sign, $\vec{M_s} = -\vec{M_l}$.

For a rigid and smooth sphere with diameter d_p, the drag force can be given by:

$$\vec{f_D} = -\frac{3}{4 d_p} C_D \rho_l \left(\vec{V_s} - \vec{V_l} \right) \left| \vec{V_s} - \vec{V_l} \right| \tag{4}$$

where C_D is the drag coefficient, d_p is the particle diameter and $(\vec{V_s} - \vec{V_l})$ is the relative velocity vector between the solid (s) and the liquid (l) phases. The drag coefficient for a spherical particle is calculated analytically by the Stokes' law for the viscous regime, $Re \ll 1$, and it is a constant value, 0.44, for the inertial regime. For a dilute solid suspension, the transition between both regimes can be computed by Schiller and Naumann (1933)

$$C_{D,\alpha_s<0.2} = \alpha_l^{-1.65} max \left[\frac{24}{Re'} \left(1 + 0.15 Re'^{0.687} \right), 0.44 \right] \tag{5}$$

and for concentrated suspensions, a most appropriate model was proposed by Gidaspow (1994),

$$C_{D,\alpha_s>0.2} = C_{(l,s)}^{(d)} \frac{4 d_p}{3 \alpha_s \rho_s \left| \vec{V_s} - \vec{V_l} \right|} \tag{6}$$

The Eq. 5 is applicable to solid volume fractions of $\alpha_s < 0.2$, while Eq. 6 is used for $\alpha_s > 0.2$. The liquid volume fraction is represented by α_l, while ρ_s is the solid-phase density, and $\vec{V_l}$ and $\vec{V_s}$ are the local liquid and solid velocities,

respectively. The effective Reynolds number, Re', is a function of the particle Reynolds number and the solid volume fraction:

$$Re' = \alpha_s Re_p \tag{7}$$

where

$$Re_p = \frac{\rho_l \left|\vec{V}_s - \vec{V}_l\right| d_p}{\mu_l} \tag{8}$$

and

$$C^{(d)}_{(l,s)} = 150\frac{(1-\alpha_l)^2 \mu_l}{\alpha_l d_p^2} + \frac{7}{4}\frac{(1-\alpha_l)\rho_l \left|\vec{V}_s - \vec{V}_l\right|}{d_p} \tag{9}$$

The virtual mass force (Ishii and Hibiki, 2010), $\vec{f}_{VM}$, is computed by using the following expression:

$$\vec{f}_{VM} = -6\rho_l C_{VM}\left[\frac{D\left(\vec{V}_s - \vec{V}_l\right)}{Dt}\right] \tag{10}$$

where C_{VM} is the virtual mass coefficient. The commonly used value of 0.5 is adopted in the current work.

The lift force (Auton, 1987), $\vec{f}_L$, is calculated by the form:

$$\vec{f}_L = -C_L\rho_l\left[(\vec{V}_s - \vec{V}_l) \times curl(\vec{V}_l)\right] \tag{11}$$

where C_L is the lift coefficient. The lift coefficient is correlated to both the particle Reynolds number, Re_p, and the vorticity Reynolds number, Re_ω, which is calculated in the current work using the expression proposed by Saffman (1965):

$$C_L = \frac{3}{2\pi\sqrt{Re_w}}C'_L \tag{12}$$

where

$$Re_\omega = \frac{\rho_l \left|\nabla \times V_l\right| d_p^2}{\mu_l} \tag{13}$$

and,

$$C'_L : \{\, 6\ .46 f\left(Re_p, Re_\omega\right) for : Re_p < 40 \qquad\qquad 0.338\left(\beta Re_p\right)^{1/2} for : 40 < Re_p < 100 \tag{14}$$

where

$$\beta = \frac{Re_\omega}{2Re_p} \tag{15}$$

and,

$$f(Re_p, Re_\omega) = (1 - 0.3314\beta^{1/2})e^{-0.1Re_p} + 0.3314\beta^{1/2} \tag{16}$$

As the Euler-Euler model treats both phases as interpenetrating continua, dynamic viscosity is required for both liquid and solid phases. In the current work, the liquid phase is assumed as a Newtonian fluid. Differently than several prior studies that assume the solid viscosity as equal to the liquid viscosity (Shi and Rzehak, 2020) or it is computed by the kinetic theory of granular flows (Yan *et al.*, 2011; Maluta *et al.*, 2019), the solid shear viscosity, μ_s, is modeled here following Enwald *et al.* (1996), who suggest that the suspension viscosity can be estimated by averaging the liquid and solid viscosities weighted by the respective volume fractions.

$$\eta_{sup} = \alpha_l\mu_l + \alpha_s\mu_s \tag{17}$$

where, η_{sup} is the suspension viscosity, α_l is the liquid volume fraction, μ_l is the liquid viscosity, α_s is the solid volume fraction and μ_s is the viscosity associated to the dispersed phase.

A useful expression (Tanner, 2018) for the suspension viscosity that is based on the work of Krieger and Dougherty (1959) is used here:

$$\eta_{sup} = \mu_l \left(1 - \frac{\alpha_s}{\alpha_{s_{pac}}}\right)^{-2} \tag{18}$$

where, $\alpha_{s_{pac}}$ is the packed solid volume fraction and is assumed equal to 0.61 in this work. As reported by (on Official Nomenclature and Symbols, 2013), the packed solid volume fraction is a measure of a statically stable packing of the particles and is not a well known quantity that could vary randomly between 0.55 to 0.64. Now, one can estimate the solid shear viscosity:

$$\alpha_s \mu_s = \eta_s = \left(\mu_l \left(1 - \frac{\alpha_s}{\alpha_{smax}}\right)^{-2} - \alpha_l \mu_l\right) \tag{19}$$

where $\alpha_s \mu_s$ is considered the solid shear viscosity related to the solid volume fraction and is given by η_s.

3. NUMERICAL APPROACH

3.1 Numerical solution

The governing equations are discretized by using the element-based finite volume method and solved by employing the CFD package ANSYS®CFX®(ANSYS Inc., 2019). A High-Resolution scheme (Yeoh and Tu, 2009) for the spatial discretization of the advection terms was adopted. The scheme is a blending between the first-order upwind and second-order central differencing schemes, taking into account the boundedness criterion of Barth and Jespersen (1989). A method developed for co-located mesh systems based on the scheme proposed by Rhie and Chow (1983) was used for the pressure-velocity coupling.

The 3D mesh composed of hexahedral structured elements for the three domain are used to solve the problem. A 1 deg extension is assumed in the azimuthal direction together with rotational periodicity conditions (ANSYS Inc., 2019), in order to save computational time. Five grid sizes are tested to verify the sensitivity of the numerical solution with respect to the mesh for all three geometries. The convergence criterion adopted was the minimization of the mean square root of the normalized residuals to a value smaller than 10^{-5} (ANSYS Inc., 2019).

It was carried out a mesh sensitivity test for two-phase flow. Fluid properties are assumed Newtonian, being the density of 840 kg m^{-3} and viscosity of 0.022 Pa s. For the dispersed phase a suspension composed of particles with a diameter of 50 μm and particle volume fraction (PVF) of α_s = 0.2 is assumed. For the CP and CC geometries, buoyancy is neglected, and two rotation speeds are considered, one for each case, Ω = 28.6 rad s^{-1} and Ω = 2.8 rad s^{-1}, respectively. The rotation speeds correspond to a shear rate of 818 s^{-1} and 33.8 s^{-1}, respectively. For PP geometry buoyancy is considered and a rotation speed of Ω = 28.6 rad s^{-1} is assumed, which corresponds to a shear rate of 500 s^{-1}.

The computed torque and the PVF profile in the radial direction are monitored to check for the grid size sensitivity. The computed torque on the cone-plate (CP), parallel-plates (PP) and on the concentric cylinders (CC) geometries were calculated on the cone surface, on the lower plate and on the internal cylinders by the Eq. 20, respectively.

$$T_{cal} = \int_0^R \tau_w(r) 2\pi r^2 dr \tag{20}$$

where τ_ω is the shear stress on the wall.

Tables 1, 2 and 3 presents the torque for each mesh and the respective percentage deviation to the torque obtained with the most refined grid in each operational condition. The calculated torque proved to be little sensitive to the mesh refinement, however, different behavior was observed regarding the PVF profile.

Table 1. Torque obtained for the five different meshes and their corresponding percentage deviations with respect to the finest mesh 5. The suspension is subject to a angular speed of 28.6 rad s^{-1}, that correspond to the shear rate of 818 s^{-1} at the edge of the plate.

Mesh	Nodes	CP Tor.susp. (Nm)	devn(%)
1	1050	4.5042×10^{-4}	0.91
2	4035	4.4790×10^{-4}	0.34
3	11970	4.4678×10^{-4}	0.09
4	24705	4.4642×10^{-4}	0.01
5	41940	4.4636×10^{-4}	-

Table 2. Torque obtained for the five different meshes and their corresponding percentage deviations with respect to the finest mesh 5. The suspension is subject to a angular speed of 28.6 rad s^{-1}, that correspond to the shear rate of 500 s^{-1} at the edge of the plate.

Mesh	Nodes	PP Tor.susp. (Nm)	devn(%)
1	1050	2.1328×10^{-4}	-2.47
2	4035	2.1896×10^{-4}	0.12
3	11970	2.1900×10^{-4}	0.14
4	24705	2.1875×10^{-4}	0.03
5	41940	2.1868×10^{-4}	-

Table 3. Torque obtained for the five different meshes and their corresponding percentage deviations with respect to the finest mesh 5. The suspension is subject to a angular speed of 28.6 rad s^{-1}, that correspond to the shear rate of 338 s^{-1} at the edge of the plate.

Mesh	Nodes	CC Tor.susp. (Nm)	devn(%)
1	36439	6.8694×10^{-5}	0.01
2	53758	6.8683×10^{-5}	-0.01
3	63990	6.8689×10^{-5}	0.00
4	75990	6.8699×10^{-5}	0.01
5	115335	6.8690×10^{-5}	-

Figure 2 a), b) and c) depict the PVF profile in the radial direction for all three geometries. The PVF was monitored in $z^* = 0.5$ all long the radius. As one can notice, the PVF profiles obtained with mesh refinement levels 1, 2 and 3 show deviations with respect to the results obtained with the most refined ones. However, profiles for Meshes 4 and 5 agree well one with each other.Thus, Mesh 4 is adopted to conduct the numerical simulations discussed in the next section.

4. RESULTS

4.1 Comparison with experimental results

A quantitative comparison with different experimental results from the literature are conducted. Moon *et al.* (2015) performed their experiments with smooth rigid spherical polystyrene particles (PS) with diameter of 80 μm and density of 1050 kg m^{-3}, dispensed in silicon oil with density of 970 kg m^{-3} and viscosity of 1.1 Pa s. They varied the volume fraction from 0.1 to 0.5 and maintained a shear rate of 10 s^{-1} at the plate edge. Zarraga *et al.* (2000) carried out experiments with glass particles with diameter of 43 μm and density of 2412 kg m^{-3}, added to a fluid with density of 1322 kg m^{-3} and viscosity of 0.252 Pa s. They changed the solid volume fraction from 0.306 to 0.501. Gamonpilas *et al.* (2016) conducted their tests with the suspension used by Moon *et al.* (2015).

Figure 3 compares the numerical values of apparent relative viscosity as a function of particle volume fraction with the three different experimental data from the literature (Zarraga *et al.*, 2000; Moon *et al.*, 2015; Gamonpilas *et al.*, 2016). Independently of the data source and despite the wide range particle volume fraction (0.1 to 0.5), fluid viscosity (0.252 to 1.1 Pa s), particle density (1.050 to 2.410 kg m^{-3}), and particle size (43 to 80 μm), the numerical values agree quiet well with the literature data.

4.2 Effect of particle volume fraction and shear rate on apparent relative viscosity in suspensions without buoyancy effect

This section presents a comparison of the apparent relative viscosity as a function of the particle volume fraction and the shear rate for three geometries. The CP geometry is composed of a cone and a plate of the same radius R (R = 17.5 mm), which form an angle of 2 degrees to each other. The second geometry is a PP of radius R (R = 17.5 mm), separated by a distance H_p (H_p = 1 mm). The CC geometry consists of two cylinders of height H_c (H_c = 37.6 mm), concentric with respect to each other and separated by a gap of 1.06 mm, which is the distance between the inner radius and the outer radius of the cylinders, R_i (R_i = 12.54 mm) and R_o (R_o = 13.60 mm), respectively.

To evaluate the effect of particle volume fraction on the apparent relative viscosity, five fractions were used, from 0.1 to 0.5. The suspensions are composed of particles with 50 μm diameter, density equal to the liquid, ρ_l = 1,020 kg m^{-3}, and liquid viscosity of 0.022 Pa s. The tests were performed at a shear rate of 10 s^{-1} and 100 hours duration. The relative viscosity results are shown in fig. 4. As expected, it is observed that the apparent relative viscosity is not dependent on geometry, and results agree quiet well with the value estimated by Eq. 18 .

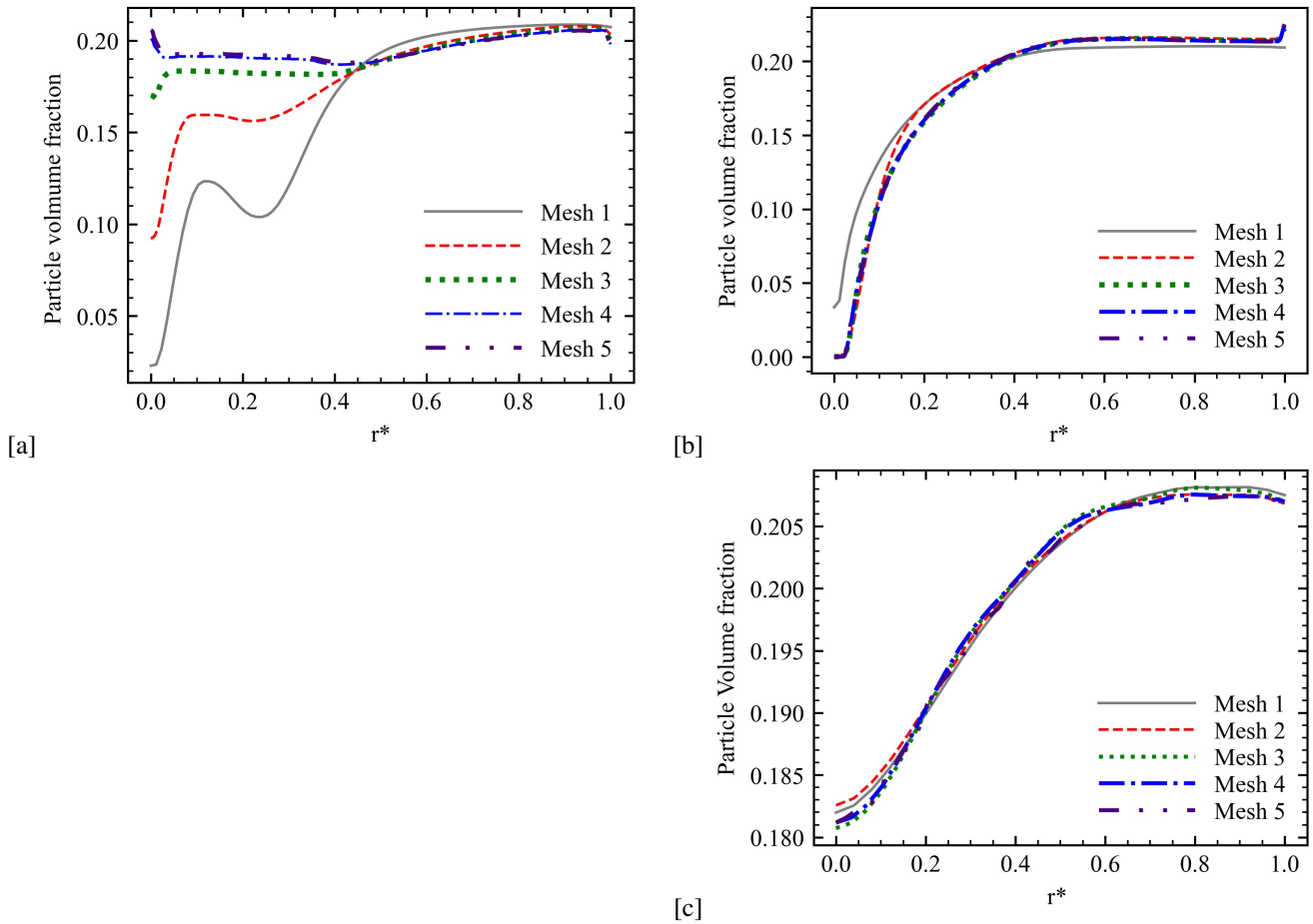

Figure 2. Particle volume fraction profiles obtained for all three geometries, for 5 mesh refinement levels each. a) Cone-plate, b) Parallel-plates and, c) Concentric cylinders.

Next, it was evaluated the effect of shear rate in a suspension with a particle volume fraction of 0.2, in three geometries. Seven shear rates were selected to carry out the study, from 0.001 s^{-1} to 500 s^{-1}. The test was run for 100 hours.

Figure 5 shows that apparent relative viscosity values for seven shear rate. It is observed that for shear rate up to 10 s^{-1}, the tests performed with CP and PP geometry did not show considerable divergence between each other. However, for CC geometry, it is observed that apparent viscosity show a slight increase in values. For higher shear rate, above 10 s^{-1}, it is observed that apparent viscosity show a slight increase for PP geometry. Even more pronounced increase is observed in the CP and CC geometries. This increase can be due to the inertia effect, as already observed by Linares-Guerrero *et al.* (2017), and suspension heterogeneity, which can also be intensified due to inertia.

To understand the effect of shear rate on the apparent relative viscosity results, it was monitored the distribution of particles in the radial direction and at $z^* = 0.5$, and in the z direction along $r^* = 0.6$ for CP and PP geometries and $r^* = 0.5$ for CC geometry. As can be seen in fig. 6, particle distribution remains almost unchanged for all geometries at shear rates up to 1 s^{-1}. Increasing shear rate, particle distribution tends to become more heterogeneous. It is observed, in fig. 6 a), CP geometry, that the particles tend to be concentrated in the central region, up to half the radius, while, a particle decrease is noted in the periphery region.

Opposite behavior is observed in fig. 6 c), PP geometry, in which the particles tend to be homogeneously distributed in the geometry, but with a slight reduction in the center. In the figure. 6 d), PP geometry, an increase in the solids fraction is observed, near the rotating plate and in the gap central region, with increase in the shear rate. In CC geometry, particle distribution tends to show greater heterogeneity in the gap region and in the cone, and this heterogeneity is the main responsible for the increase in the apparent relative viscosity value.

Figure 6 a) shows CP geometry. The image depicts an increase in particle volume fraction in the cone truncation region at the end of the simulation, however, the particles initially accumulate near the region with the physical restriction and over time tend to migrate to the region closer to the center of the geometry. Apparently, this increase in the particle volume fraction is related only to the physical constraint imposed by the geometry, since no other mechanism was observed that would enable to increase particles near the center of the geometry. Figure 6 c) shows the PP geometry. It can be noticed a small decrease in particle volume fraction in the center of the geometry, and a slight increase in the periphery region. This slight heterogeneity is due to the drag force that acts in the radial direction and with greater intensity near the plate that is

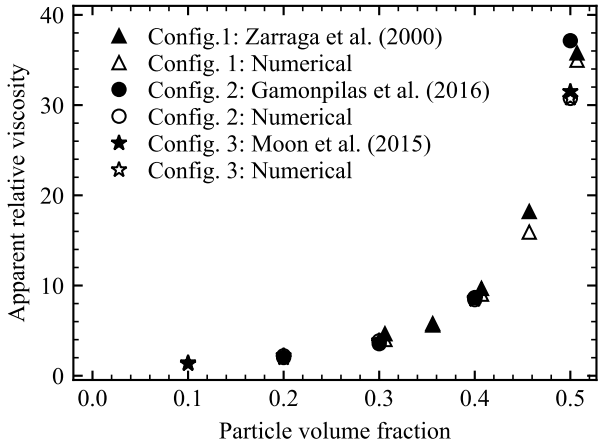

Figure 3. Relative viscosity obtained for different particle volume fraction from experimental Zarraga *et al.* (2000); Moon *et al.* (2015); Gamonpilas *et al.* (2016) and numerical results.

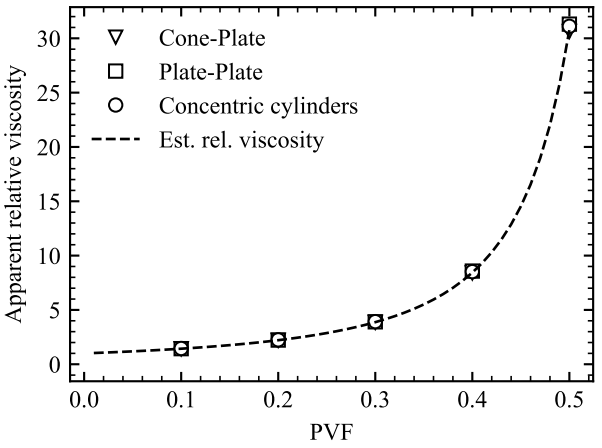

Figure 4. Comparison of apparent relative viscosity as a function of particle volume fraction (PVF) for three geometries. The geometries evaluated are Cone-Plate (CP), Plate-Plate (PP) and Concentric Cylinders (CC). Five particle volumetric fractions were evaluated, from 0.1 to 0.5, with shear rate of 10 s^{-1}. The suspensions are composed by particles with 50 μm diameter, density equal to the liquid, ρ_l = 1,020 kg m^{-3}, and liquid viscosity of 0.022 Pa s.

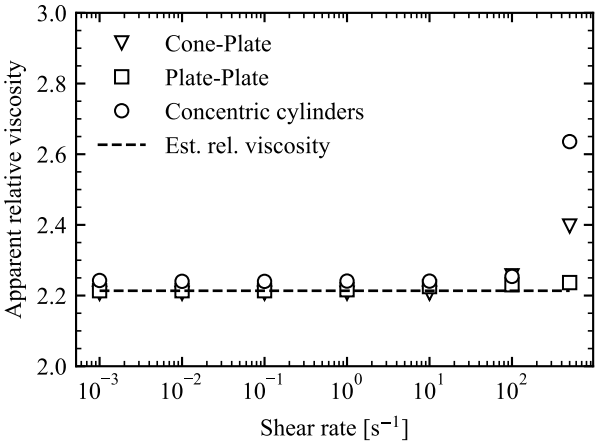

Figure 5. Comparison of apparent relative viscosity as a function of shear rate for three geometries. The evaluated geometries are Cone-Plate (CP), Plate-Plate (PP) and Concentric Cylinders (CC). The suspension, α_s = 0.2, is composed of particle diameter of 50 μm, with the same density of the liquid, ρ_l = 1,020 kg m^{-3}, and the liquid viscosity is 0.022 Pa s. The evaluated shear rates are: 0.001, 0.01, 0.1, 1, 10, 100 and 500 s^{-1}.

rotating compared to the plate that is stationary. As a result, particles are dragged to the periphery of the plate. Particle distribution relative to CC geometry is show in fig. 6 f). Note that the particle distribution tends to be heterogeneous along

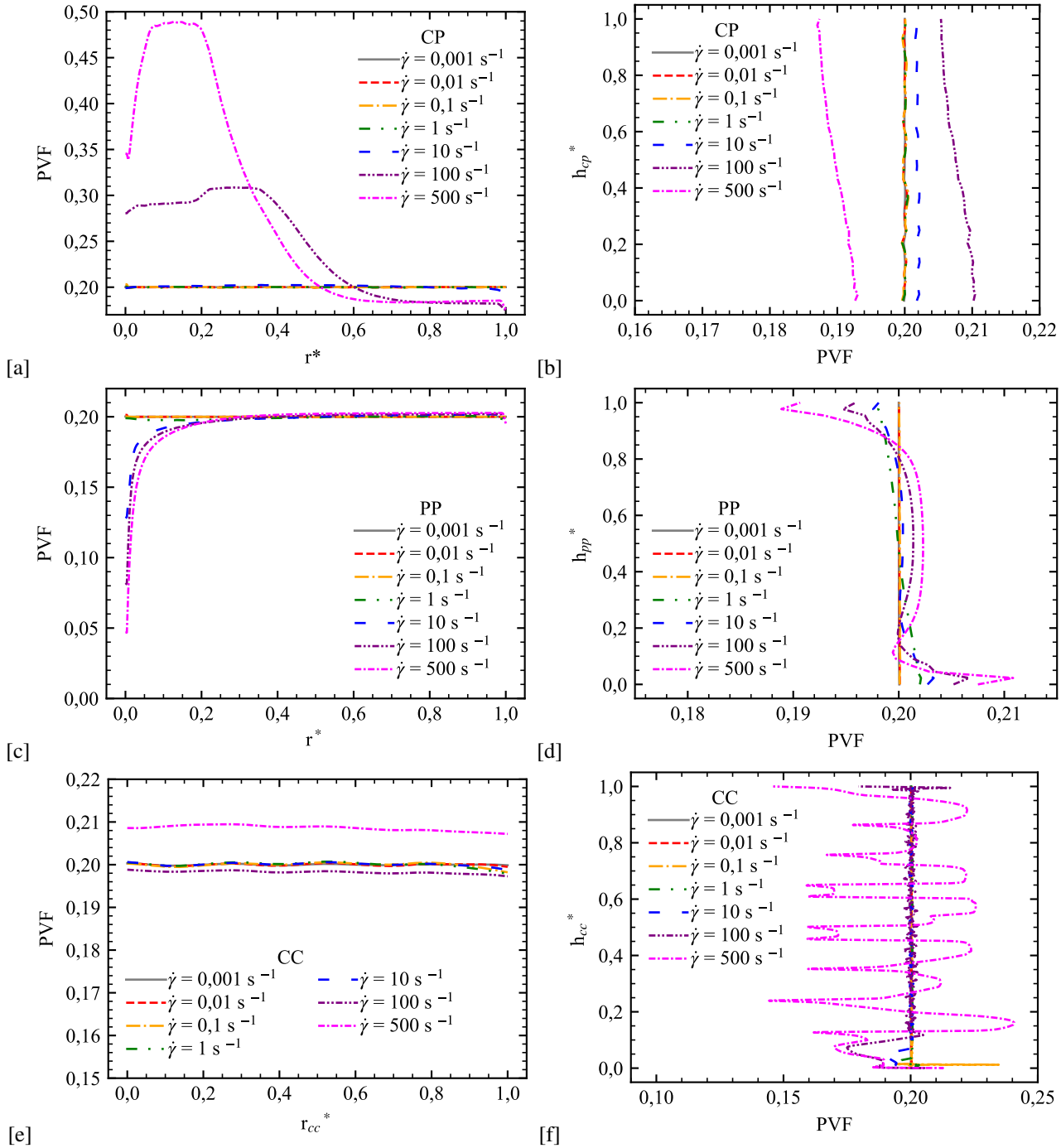

Figure 6. Particle distribution profile in the radial direction and in the z direction of the suspension mentioned in fig. 5. a) represents the particle distribution profile in the radial direction and at $z^* = 0.5$ for the CP geometry. b) represents the particle distribution profile in the z direction and at $r^* = 0.6$ for the CP geometry. c) represents particle distribution profile in the radial direction and at $z^* = 0.5$ for the PP geometry. d) represents the particle distribution profile in the z direction and at $r^* = 0.6$ for the PP geometry. e) represents the particle distribution profile in the radial direction and at $z^* = 0.5$ for the CC geometry. f) represents the particle distribution profile in the z direction and at $r^* = 0.5$ for CC geometry.

the entire geometry. At the bottom of the concentric cylinders there is a cone-plate coupled, it is observed, in this region, the same behavior observed for the CP geometry. However, in the gap region, it can be observed a great heterogeneity that is the main responsible to increase apparent viscosity.

5. CONCLUSIONS

The non-colloidal suspension rheometric flow are numerically investigated. The two-fluid approach is mainly used to model the suspension particle motion and to evaluate its consequence on the measured viscosity. From the numerical results, it was observed that the apparent viscosity is affected by particle distribution. It was also noted that the apparent viscosity is insensitive to the geometry at low shear rates. However, when the shear rate is increased the apparent viscosity is affected by the geometry configuration. Parallel-plate geometry shown the smallest divergence on apparent relative viscosity as function of shear rate.

6. ACKNOWLEDGEMENTS

The authors also thank the Multilab LabReoCERNN/UTFPR for providing the Rheometers used in the current work.

7. REFERENCES

Abbott, J., Tetlow, N., Graham, A., Altobelli, S., Fukushima, E., Mondy, L. and Stephens, T., 1991. "Experimental observations of particle migration in concentrated suspensions: Couette flow". *Journal of rheology*, Vol. 35, No. 5, pp. 773–795.

Acrivos, A., Mauri, R. and Fan, X., 1993. "Shear-induced resuspension in a couette device". *International journal of multiphase flow*, Vol. 19, No. 5, pp. 797–802.

ANSYS Inc., 2019. "CFX-Solver Manager User's Guide".

Auton, T., 1987. "The lift force on a spherical body in a rotational flow". *Journal of fluid Mechanics*, Vol. 183, pp. 199–218.

Barth, T. and Jespersen, D., 1989. "The design and application of upwind schemes on unstructured meshes". In *27th Aerospace sciences meeting*. p. 366.

Chapman, B. and Leighton Jr, D., 1991. "Dynamic viscous resuspension". *International journal of multiphase flow*, Vol. 17, No. 4, pp. 469–483.

Chow, A.W., Sinton, S.W., Iwamiya, J.H. and Stephens, T.S., 1994. "Shear-induced particle migration in couette and parallel-plate viscometers: Nmr imaging and stress measurements". *Physics of Fluids*, Vol. 6, No. 8, pp. 2561–2576.

Dai, S.C., Bertevas, E., Qi, F. and Tanner, R.I., 2013. "Viscometric functions for noncolloidal sphere suspensions with newtonian matrices". *Journal of Rheology*, Vol. 57, No. 2, pp. 493–510.

Denn, M.M. and Morris, J.F., 2014. "Rheology of non-brownian suspensions". *Annual review of chemical and biomolecular engineering*, Vol. 5, pp. 203–228.

Denn, M.M., Morris, J.F. and Bonn, D., 2018. "Shear thickening in concentrated suspensions of smooth spheres in newtonian suspending fluids". *Soft matter*, Vol. 14, No. 2, pp. 170–184.

Eckstein, E.C., Bailey, D.G. and Shapiro, A.H., 1977. "Self-diffusion of particles in shear flow of a suspension". *Journal of Fluid Mechanics*, Vol. 79, No. 1, pp. 191–208.

Enwald, H., Peirano, E. and Almstedt, A.E., 1996. "Eulerian two-phase flow theory applied to fluidization". *International Journal of Multiphase Flow*, Vol. 22, pp. 21–66.

Fall, A., Lemaitre, A., Bertrand, F., Bonn, D. and Ovarlez, G., 2010. "Shear thickening and migration in granular suspensions". *Physical review letters*, Vol. 105, No. 26, p. 268303.

Gamonpilas, C., Morris, J.F. and Denn, M.M., 2016. "Shear and normal stress measurements in non-brownian monodisperse and bidisperse suspensions". *Journal of Rheology*, Vol. 60, No. 2, pp. 289–296.

Gidaspow, D., 1994. *Multiphase flow and fluidization: continuum and kinetic theory descriptions*. Academic press.

Huang, N. and Bonn, D., 2007. "Viscosity of a dense suspension in couette flow". *Journal of fluid mechanics*, Vol. 590, pp. 497–507.

Husband, D. and Gadala-Maria, F., 1987. "Anisotropic particle distribution in dilute suspensions of solid spheres in cylindrical couette flow". *Journal of Rheology*, Vol. 31, No. 1, pp. 95–110.

Husband, D., Mondy, L., Ganani, E. and Graham, A., 1994. "Direct measurements of shear-induced particle migration in suspensions of bimodal spheres". *Rheologica acta*, Vol. 33, No. 3, pp. 185–192.

Ishii, M. and Hibiki, T., 2010. *Thermo-fluid dynamics of two-phase flow*. Springer Science & Business Media.

Kim, J.M., Lee, S.G. and Kim, C., 2008. "Numerical simulations of particle migration in suspension flows: Frame-invariant formulation of curvature-induced migration". *Journal of Non-Newtonian Fluid Mechanics*, Vol. 150, No. 2-3, pp. 162–176.

Konijn, B., Sanderink, O. and Kruyt, N.P., 2014. "Experimental study of the viscosity of suspensions: Effect of solid fraction, particle size and suspending liquid". *Powder technology*, Vol. 266, pp. 61–69.

Krieger, I.M. and Dougherty, T.J., 1959. "A mechanism for non-newtonian flow in suspensions of rigid spheres". *Transactions of the Society of Rheology*, Vol. 3, No. 1, pp. 137–152.

Krishnan, G.P., Beimfohr, S. and Leighton, D.T., 1996. "Shear-induced radial segregation in bidisperse suspensions".

Journal of Fluid Mechanics, Vol. 321, pp. 371–393.

Kulkarni, P.M. and Morris, J.F., 2008. "Suspension properties at finite reynolds number from simulated shear flow". *Physics of Fluids*, Vol. 20, No. 4, p. 040602.

Leighton, D. and Acrivos, A., 1987. "The shear-induced migration of particles in concentrated suspensions". *Journal of Fluid Mechanics*, Vol. 181, pp. 415–439.

Lewis, T. and Nielsen, L., 1968. "Viscosity of dispersed and aggregated suspensions of spheres". *Transactions of the Society of Rheology*, Vol. 12, No. 3, pp. 421–443.

Linares-Guerrero, E., Hunt, M.L. and Zenit, R., 2017. "Effects of inertia and turbulence on rheological measurements of neutrally buoyant suspensions". *Journal of Fluid Mechanics*, Vol. 811, pp. 525–543.

Liu, W. and Wu, C.Y., 2019. "Analysis of inertial migration of neutrally buoyant particle suspensions in a planar poiseuille flow with a coupled lattice boltzmann method-discrete element method". *Physics of Fluids*, Vol. 31, No. 6, p. 063301.

Majji, M.V. and Morris, J.F., 2018. "Inertial migration of particles in taylor-couette flows". *Physics of Fluids*, Vol. 30, No. 3, p. 033303.

Maluta, F., Paglianti, A. and Montante, G., 2019. "Rans-based predictions of dense solid–liquid suspensions in turbulent stirred tanks". *Chemical Engineering Research and Design*, Vol. 147, pp. 470–482.

Matas, J.P., Morris, J.F. and Guazzelli, É., 2004. "Inertial migration of rigid spherical particles in poiseuille flow". *Journal of Fluid Mechanics*, Vol. 515, pp. 171–195.

Merhi, D., Lemaire, E., Bossis, G. and Moukalled, F., 2005. "Particle migration in a concentrated suspension flowing between rotating parallel plates: Investigation of diffusion flux coefficients". *Journal of Rheology*, Vol. 49, No. 6, pp. 1429–1448.

Moon, J.Y., Dai, S., Chang, L., Lee, J.S. and Tanner, R.I., 2015. "The effect of sphere roughness on the rheology of concentrated suspensions". *Journal of Non-Newtonian Fluid Mechanics*, Vol. 223, pp. 233–239.

Morris, J.F. and Boulay, F., 1999. "Curvilinear flows of noncolloidal suspensions: The role of normal stresses". *Journal of rheology*, Vol. 43, No. 5, pp. 1213–1237.

Mueller, S., Llewellin, E. and Mader, H., 2009. "The rheology of suspensions of solid particles". *Proceedings of the Royal Society A: Mathematical, Physical and Engineering Sciences*, Vol. 466, No. 2116, pp. 1201–1228.

Nott, P.R. and Brady, J.F., 1994. "Pressure-driven flow of suspensions: simulation and theory". *Journal of Fluid Mechanics*, Vol. 275, pp. 157–199.

on Official Nomenclature, A.H.C. and Symbols, 2013. "Official symbols and nomenclature of the society of rheology". *Journal of Rheology*, Vol. 57, No. 4, pp. 1047–1055.

Pednekar, S., Chun, J. and Morris, J.F., 2018. "Bidisperse and polydisperse suspension rheology at large solid fraction". *Journal of Rheology*, Vol. 62, No. 2, pp. 513–526.

Rhie, C. and Chow, W.L., 1983. "Numerical study of the turbulent flow past an airfoil with trailing edge separation". *AIAA journal*, Vol. 21, No. 11, pp. 1525–1532.

Saffman, P., 1965. "The lift on a small sphere in a slow shear flow". *Journal of fluid mechanics*, Vol. 22, No. 2, pp. 385–400.

Schiller, L. and Naumann, A., 1933. "Fundamental calculations in gravitational processing". *Zeitschrift Des Vereines Deutscher Ingenieure*, Vol. 77, pp. 318–320.

Shauly, A., Wachs, A. and Nir, A., 1998. "Shear-induced particle migration in a polydisperse concentrated suspension". *Journal of Rheology*, Vol. 42, No. 6, pp. 1329–1348.

Shi, P. and Rzehak, R., 2020. "Solid-liquid flow in stirred tanks: Euler-euler/rans modeling". *Chemical Engineering Science*, p. 115875.

Tanner, R.I., 2018. "Aspects of non-colloidal suspension rheology". *Physics of Fluids*, Vol. 30, No. 10, p. 101301.

Tanner, R.I., 2020. "Computation and experiment in non-colloidal suspension rheology". *Journal of Non-Newtonian Fluid Mechanics*, p. 104282.

Tanner, R.I. and Dai, S., 2016. "Particle roughness and rheology in noncolloidal suspensions". *Journal of Rheology*, Vol. 60, No. 4, pp. 809–818.

Tehrani, M., 1996. "An experimental study of particle migration in pipe flow of viscoelastic fluids". *Journal of Rheology*, Vol. 40, No. 6, pp. 1057–1077.

Wang, Y., Mauri, R. and Acrivos, A., 1996. "The transverse shear-induced liquid and particle tracer diffusivities of a dilute suspension of spheres undergoing a simple shear flow". *Journal of fluid mechanics*, Vol. 327, pp. 255–272.

Yan, W.C., Shi, D.P., Luo, Z.H. and Lu, Y.H., 2011. "Three-dimensional cfd study of liquid–solid flow behaviors in tubular loop polymerization reactors: The effect of guide vane". *Chemical engineering science*, Vol. 66, No. 18, pp. 4127–4137.

Yeoh, G. and Tu, J., 2009. *Modelling subcooled boiling flows*. Nova Science Publishers, Inc.

Yeoh, G.H. and Tu, J., 2019. *Computational techniques for multiphase flows*. Butterworth-Heinemann.

Zarraga, I.E., Hill, D.A. and Leighton Jr, D.T., 2000. "The characterization of the total stress of concentrated suspensions of noncolloidal spheres in newtonian fluids". *Journal of Rheology*, Vol. 44, No. 2, pp. 185–220.

8. RESPONSIBILITY NOTICE

The following text, properly adapted to the number of authors, must be included in the last section of the paper: The author(s) is (are) solely responsible for the printed material included in this paper.